ORIGINAL PAPER

Exciton propagation via quantum walks based on non-Hermitian coin flip operations

A. Thilagam

Abstract We examine the coherent propagation of the one-dimensional Frenkel exciton (correlated electron-hole pair system) based on a model of a quantum walker in multi-dimensional Hilbert space. The walk is governed by a non-Hermitian coin flip operation coupled to a generalized shift process. The dissipative coin flip operation is associated with amplitude leakages at occupied sites, typical of processes which occur when an exciton is transferred along dimer sites in photosynthetic protein complexes. We analyze the characteristics probability distribution of the one-dimensional quantum walk for various system parameters, and examine the complex interplay between non-Markovian signatures and amplitude leakages within the Hilbert position subspace. The visibility of topological defects such as exceptional points, and non-Markovian signatures via quantum tomography based spectroscopic measurements is discussed.

Keywords Frenkel exciton · Quantum walk · Photosynthetic protein complexes · Entropy · Quantum tomography · Non-Markovian signatures

1 Introduction

It is well known that systems which enable quantum walks of one or more propagating entities (quasi-particle or excitation) exhibit intriguing features not seen in the classical walker [1–6]. For instance, the quantum walker moves away faster from the point of initial start than the classical random walker. Several works [7–9] have shown that the quantum information encoded in the walker's positions provide a basis for universal quantum computation, even allowing single-qubit measurements to be incorporated

A. Thilagam (✉)
Information Technology, Engineering and Environment,
University of South Australia, Adelaide, SA 5095, Australia
e-mail: thilaphys@gmail.com

with localized operators and existing quantum error-correcting codes [8]. Quantum walks can be modeled either as continuous-time quantum walk (CTQW) [5] or as discrete-time quantum walk (DTQW) [2,10,11]. While the system evolves with no restriction on time during CTQW, the DTQW involves an entangled system of a walker and a coin, and an evolution operator which is applied to both systems in discrete time steps. In both the CTQW and DTQW models, the quantum walker moves along discrete points within the confines of undirected graphs.

Since the inception of the basic model of a sole walker moving left or right simultaneously, and conditional on the two outcomes of a flipped quantum coin, several variants of the DTQW have been proposed. One known model is based on multiple walkers and coins [12–14], the second, centers on the presence of a distinguished node due to local change of phase [15], while a third DTQW variant involves quantum walks in the presence of traps [16]. A non-Hermitian coin toss model has also been considered on lattices and finite graphs, incorporating the behavior of open quantum systems [17]. Quantum walks can be categorized depending on the behavior of the spreading measure σ in the long time limit, accordingly the walk can be ballistic ($\sigma \propto t$), diffusive ($\sigma \propto \sqrt{t}$) or localized ($\sigma \propto$ const) [18–20]. Quantum walks have been demonstrated using single photons in space, with walks up to six steps measured, and the quantum-to-classical transition analyzed via the decoherence mechanism [21]. Another study [22] examined the simulations of quantum walks via confinement of a single Mg^+ ion in a linear Paul trap. Recently [23] quantum walks were performed on an integrated array of symmetric, polarization insensitive, directional couplers in which two-photon polarization entangled states were introduced. The dynamics of symmetric and antisymmetric particles undergoing quantum walks was demonstrated experimentally by utilizing the different statistics of singlet and triplet entangled states [23].

The various modifications and categorization of quantum walks provide useful techniques in simulating realistic systems such as photosynthetic protein complexes [24–31] which convert solar energy into chemical energy through extremely efficient propagation schemes. The energy of photons absorbed by a intricate network of bacteriochlorophylls is transferred, with almost near unity quantum efficiency to a reaction center (RC) where energy conversion and charge separation occurs. The well-known Fenna-Mathews-Olson (FMO) pigment protein complex acts an interface between the chlorosomic antenna and the reaction center in the green sulphur bacteria [25,26]. The FMO interface constitutes eight coupled bacteriochlorophyll-a chromophores (BChl a) that gives rise to eight excitonic states which perform the vital role of transferring energy from the antennae end toward the reaction center.

Various theories [28,29,31–37] have been proposed in recent years to account for the high efficiencies of energy transfer in the FMO protein complex. Ishizaki et. al. [31] showed that quantum coherence allows excitations to propagate without being trapped at sites with lower energies, while the role of a critical ratio in quantum coherence and environmental noise in achieving optimal functionality and efficiency in photosynthetic systems was examined in other works [28,29,37]. In an earlier work, we demonstrated that quantum information processing tasks involving teleportation and decodification based on specific states (W-like states) of the FMO complex may contribute to coherent oscillations at physiological temperatures [34]. Recently, we con-

sidered the importance of the Zeno mechanism-non-Markovianity link [38] in wider networked molecular systems of photosynthetic membrane surfaces that constitute thousands of bacteriochorophylls. While protein-induced (time-dependent) fluctuations and dissipation play an important role in controlling the energy transfer dynamics in photosynthetic pigment-protein complexes, propagation schemes based on quantum coherence has gained attention in recent years [28,29,35–37]. The observations of long-lasting coherence at ambient temperatures [24] remains to be fully accounted for, either by semi-classical or quantum approaches, or a combination of both. Accordingly, the exact details of the link between the robust Coherent oscillations and the ultrafast times taken for excitation energy to be transferred from the antenna to the reaction center in the Fenna-Matthews-Olson trimer remains largely unidentified.

One approach that remains to be fully exploited in relation to the examination of the long-lasting coherences in light-harvesting systems, involves the non-equilibrium dynamics of non-Hermitian components in open quantum dissipative systems. The presence of non-Hermitian attributes gives rise to the characteristic features of quantum states with finite lifetimes, and quasi-bound state resonances that are present in the continuum partition. In the conventional Hermitian case, states remain un-coupled to the continuum states, and possess infinitely long lifetimes. The real and imaginary components of the non-Hermitian eigenfunctions evolve almost independently of each other during avoided level crossing [39]. These components also give rise to dynamical phase transitions that involves a bifurcation of the time scales corresponding to the lifetimes of the resonance states. The phase transitions arising from changes in environmental parameters are linked to topological defects known as exceptional points. The salient feature of short-lived and long-lived quantum states arising from non-Hermitian dynamics has important consequences for the non-ideal exciton arising from the Pauli exclusion between electrons and holes [40]. Pauli exclusion processes operate independently of the widely known coulomb processes in interacting fermion systems, and contribute to hermiticity of excitonic Hamiltonians. The non-ideal bosonic features of excitons was examined using a non-Hermitian open quantum system approach recently [41], where it was shown that long-lived quantum coherence in photosynthetic complexes may be assisted by small bosonic deviation measures. Moreover the involvement of a higher number of excitons during energy exchanges could help realize a highly correlated molecular environment.

In this work, we examine the characteristics of a one-dimensional quantum walk where there is possibility of loss of amplitude at newly located site due to a non-Hermitian coin flip operation. The leakages in excitonic occupation probabilities can be attributed to a combination of factors such as those arising from dissipation due to exciton-phonon interactions, exciton-exciton annihilation, presence of trapping centers and the ubiquitous presence of Pauli interactions as a result of the composite nature of excitonic systems [42]. In connection with the quantum walk on molecular sites, we focus on two signatures of exciton dynamics that can be derived from a quantum information theoretic approach to spectroscopic experiments. The first relates to the appearance of topological defects (exceptional points) due to coalescing of operator eigenvalues at specific values of the system parameters. The second feature relates to non-Markovian dynamics that arise at short time-scales or stronger system-environment couplings, resulting in violation of complete positivity of the

density matrix of the probed quantum system. The detection of these features have importance in the relatively new field of quantum process tomography (QPT) [43–46] where the quantum state amplitudes in the Hilbert space are obtained via a time-series of frequency-frequency correlation spectroscopic results.

This paper is organized as follows. In Sect. 2, we analyze the quantum walk on a line with a non-dissipative coin operator coupled to a generalized shift operation, and examine the probability distribution profile with respect to system parameters. In Sect. 3, we extend the problem to include the quantum walk based on a non-Hermitian coin flip operation which is used to examine the propagation of exciton in a simple one-dimensional system in Sect. 4. This model has relevance in light-harvesting systems as well as other bio-molecular networks such as J-aggregates. The characteristic features of the probability distribution with respect to changes in the waiting time τ (either walk or wait time) and λ (dissipative measure) is analyzed with respect to the total number of steps taken by the quantum walker. A discussion of the implementation of the non-Hermitian coin flip operation via the exciton spin state is provided in Sect. 4.1 and the influence of the dissipative measure λ on the Von Neumann entropy is analyzed in Sect. 4.2. In the final Sect. 5, we briefly review recent studies of quantum process tomography of relevance to excitonic systems, and present results associated with two signatures of exciton dynamics: (1) exceptional points, and (2) non-Markovianity. Section 6 provides our summary and some conclusions.

2 Basics of the discrete-time quantum walk

The one-dimensional discrete time quantum walk takes place in the total Hilbert space, $\mathcal{H}_w = \mathcal{H}_p \otimes \mathcal{H}_c$ where $\mathcal{H}_p$ ($\mathcal{H}_c$) denotes the position (coin) Hilbert space. $\mathcal{H}_p$ is spanned by the basis states $|m_p\rangle$ of the walker, $\mathcal{H}_P = \text{Span}\{|m\rangle| \ m \in Z\}$ while $\mathcal{H}_c$ is spanned by the coin states $|1_c\rangle$, $|0_c\rangle$. A conditional shift operator is employed such that the walker shifts one step forward if the linked coin state occupies a specific basis state (e.g. $|0_c\rangle$), or one step backwards if the coin state occupies the alternative basis state (e.g. $|1_c\rangle$). The operator which acts on the total Hilbert space, $\mathcal{H}_w$ for a quantum walk involving a single step is given by the propagator,

$$\hat{U} = \hat{S} \cdot \left(\hat{\mathbb{I}}_p \otimes \hat{C} \right). \tag{1}$$

where $\hat{\mathbb{I}}_p$ is the unit operator that acts on $\mathcal{H}_P$. A typical displacement operator $\hat{S}$ has the form

$$\hat{S} = \sum_{m=-\infty}^{+\infty} |(m+1)_p\rangle\langle m_p| \otimes |0_c\rangle\langle 0_c| + \sum_{m=-\infty}^{+\infty} |(m-1)_p\rangle\langle m_p| \otimes |1_c\rangle\langle 1_c|. \tag{2}$$

Prior to the application of the displacement $\hat{S}$, a coin flip operator $\hat{C}$ that acts on $\mathcal{H}_C$ is applied. $\hat{C}$ may be an arbitrary unitary operator of the form

$$\hat{C}(\alpha) = \begin{bmatrix} \alpha & \sqrt{1-\alpha^2} \\ \sqrt{1-\alpha^2} & -\alpha \end{bmatrix}. \tag{3}$$

where $\alpha = \frac{1}{\sqrt{2}}$ is associated with the well known Hadamard walk. The discrete quantum walk after t steps is given by

$$|\Psi\rangle_t = (\hat{U})^t |0_p\rangle \otimes |0_c\rangle, \tag{4}$$

where $|0_p\rangle(|0_c\rangle)$ denote the initial state of the quantum walker (coin).

In this work, we consider a generalized shift operation where

$$|0_c, m_p\rangle \rightarrow \frac{1}{\sqrt{2}} |0_c, (m-1)_p\rangle + \frac{1}{\sqrt{2}} |1_c, m_p\rangle, \tag{5}$$

$$|1_c, m_p\rangle \rightarrow -\frac{1}{\sqrt{2}} |0_c, m_p\rangle + \frac{1}{\sqrt{2}} |1_c, (m+1)_p\rangle. \tag{6}$$

The action of $\hat{C}(\alpha)$ [Eq. (3)] in the propagator $\hat{U}$ [Eq. (1)] will produce a first step configuration from an initial state, $|0_c, 0_p\rangle$, as follows

$$|0_c, 0_p\rangle \longrightarrow -\frac{\sqrt{1-\alpha^2}}{\sqrt{2}} |0_c, 0_p\rangle + \frac{\sqrt{1-\alpha^2}}{\sqrt{2}} |1_c, 1_p\rangle + \frac{\alpha}{\sqrt{2}} |0_c, -1_p\rangle$$
$$+ \frac{\alpha}{\sqrt{2}} |1_c, 0_p\rangle \tag{7}$$

After two steps, the initial configuration changes to

$$|0_c, 0_p\rangle \longrightarrow \quad \frac{1}{2}\alpha^2 |0_c, -2_p\rangle + (1 - \frac{1}{2}\alpha^2) |0_c, 0_p\rangle + \frac{1}{2}\alpha^2 |1_c, -1_p\rangle$$
$$- \frac{1}{2}\alpha^2 |1_c, 1_p\rangle - \frac{1}{2}\alpha\sqrt{1-\alpha^2} |0_c, -1_p\rangle + \frac{1}{2}\alpha\sqrt{1-\alpha^2} |0_c, 1_p\rangle$$
$$+ \frac{1}{2}\alpha\sqrt{1-\alpha^2} |1_c, 0_p\rangle - \frac{1}{2}\alpha\sqrt{1-\alpha^2} |1_c, 2_p\rangle \tag{8}$$

The expression for the distribution profile of the quantum walk becomes longer with increasing number of steps. For the one- and two- step cases [Eqs. (7), (8)], it can be easily verified that the sum of probabilities of occupation at all sites equals unity. In general this rule applies to any number of steps taken by the walker, provided there is absence of dissipation at the occupied sites. In Fig. 1, we note the spreading out of the probability distribution, typified by two counter-propagating dissimilar peaks, with increase in α which controls the coin operator in Eq. (3). The probability distribution peaks increase in height as α decreases. Due to the constructive and destructive interference features of a quantum walk, the position coordinate spreads out faster in time compared to the classical random walk, as is well known. A symmetrical profile in the probability distribution can be obtained by changing the initial state, $|0_c, 0_p\rangle$ to initial

Fig. 1 Probability distribution of a quantum walk as function of position and α obtained after 50 steps, and based on the coin operator in Eq. (3)
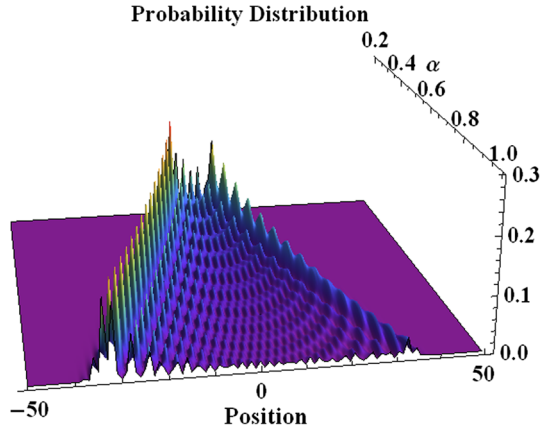
state, $\frac{1}{\sqrt{2}}(\left|0_c, 0_p\right\rangle + i \left|1_c, 0_p\right\rangle)$. In the next section, we consider a non-Hermitian walk where there is loss of amplitude at a newly occupied site.

3 Quantum walk based on a non-Hermitian coin flip operation

We consider the non-Hermitian coin flip operator $\hat{C}'$ of the following form

$$\hat{C}'(\alpha) = \begin{bmatrix} \alpha_1 & \alpha_2 \\ \alpha_2 & -\alpha_1 \end{bmatrix}. \tag{9}$$

where $\alpha_2 < \alpha_1$ and $\alpha_1^2 + \alpha_2^2 < 1$, with the difference $\Delta = \alpha_1 - \alpha_2$ determined by parameters specific to the system undergoing non-Hermitian dynamics. The action of $\hat{C}'$ in the propagator $\hat{U}$ [Eq. (1)] will produce a first step configuration from an initial state, $\left|0_c, 0_p\right\rangle$, as follows

$$\left|0_c, 0_p\right\rangle \longrightarrow \frac{\alpha_1 \left|0_c, -1_p\right\rangle}{\sqrt{2}} - \frac{\alpha_2 \left|0_c, 0_p\right\rangle}{\sqrt{2}} + \frac{\alpha_1 \left|1_c, 0_p\right\rangle}{\sqrt{2}} + \frac{\alpha_2 \left|1_c, 1_p\right\rangle}{\sqrt{2}} \tag{10}$$

where the sum of probabilities of occupation at all possible sites after one step, $N_1 = (\alpha_1^2 + \alpha_2^2)$. After two steps, the initial configuration changes to

$$\begin{aligned}
\left|0_c, 0_p\right\rangle \longrightarrow \ & \frac{1}{2}\alpha_1^2 \left|0_c, -2_p\right\rangle + (\frac{1}{2}\alpha_1^2 + \alpha_2^2) \left|0_c, 0_p\right\rangle \\
& + \frac{1}{2}\alpha_1^2 \left|1_c, -1_p\right\rangle - \frac{1}{2}\alpha_1^2 \left|1_c, 1_p\right\rangle \\
& - \frac{1}{2}\alpha_2\alpha_1 \left|0_c, -1_p\right\rangle + \frac{1}{2}\alpha_2\alpha_1 \left|0_c, 1_p\right\rangle \\
& + \frac{1}{2}\alpha_2\alpha_1 \left|1_c, 0_p\right\rangle - \frac{1}{2}\alpha_2\alpha_1 \left|1_c, 2_p\right\rangle
\end{aligned} \tag{11}$$

where the sum of probabilities of occupation at all possible sites after two steps, $N_2 = (\alpha_1^2 + \alpha_2^2)^2$. The expression for N_m for the general m steps decreases monotonically with increase in m for $\alpha_2 < \alpha_1$ as $N_m = (\alpha_1^2 + \alpha_2^2)^m$.

The form of the multipartite state in the total Hilbert space, $\mathcal{H}_p \otimes \mathcal{H}_c$, is dependent on the coefficients α_1, α_2 and the number of steps taken by the walker. We briefly examine the density matrix in the coin Hilbert space after three steps ($N = 3$) as the higher step cases involve longer expressions. By tracing out the position states of the walker, we obtain a reduced density matrix describing the quantum walk in the basis $(|0_c\rangle, |1_c\rangle)$

$$
\rho_c(\alpha_1, \alpha_2) = \begin{pmatrix} \frac{1}{4} \left(\alpha_1^2 + \alpha_2^2\right)\left(3\alpha_1^4 + 8\alpha_2^2\alpha_1^2 + 2\alpha_2^4\right) & \frac{1}{4}\alpha_1\alpha_2^3 \left(\alpha_1^2 - 4\alpha_2^2\right) \\ \frac{1}{4}\alpha_1\alpha_2^3 \left(\alpha_1^2 - 4\alpha_2^2\right) & \frac{1}{4} \left(\alpha_1^2 + \alpha_2^2\right)\left(\alpha_1^4 + 2\alpha_2^4\right) \end{pmatrix}
$$

(12)

For the simple case of $\alpha_1 = \alpha_2 = \frac{1}{\sqrt{2}}$, we get unit trace with non-negative eigenvalues, $(0.82626, 0.17374)$. For the case of $\alpha_1 = r; \alpha_2 = \sqrt{1-r^2}$, we again obtain non-negative eigenvalues, $e_1 = \frac{1}{4}(2 - f(r), e_2 = \frac{1}{4}(2 + f(r))$ where $f(r) = [r^2 \left(-25r^{10} + 115r^8 - 202r^6 + 169r^4 - 72r^2 + 16\right)]^{1/2}$, thus $e_1 + e_2 = 1$. However for the dissipative scenario where $\alpha_1 = r; \alpha_2 = \sqrt{1 - r^2 - t}$, we obtain $e_1 + e_2 = \left(1 - t^3 + 3t^2 - 3t\right)$ which decreases monotonically with increase in t. The sum of the eigenvalues of reduced density operator may used as a rough indicator of whether the trajectories of the quantum walker has indeed a physically realistic interpretation.

4 Exciton transport and the dissipative non-Hermitian coin flip operation

The propagation of the exciton (electron-hole pair system) is generally not strictly one-dimensional in light-harvesting and other bio-molecular systems such as J-aggregates, as evidenced in the volume of space transversed by the excitation. In the coherent transport model, the exciton moves as a superposition of delocalized excitations over the crystal space as an extended entangled system, and accounts well for the large free exciton path taken during coherent migration. In this case, the exciton propagation mechanism may be viewed as similar to that of a quantum walker on a graph where each vertex point represents a lattice site [47], with propagation route determined by the edge joining one vertex to another, Obviously, the number of edges incident on a specific vertex is considerably simplified for one-dimensional systems. It is possible to single out a particular vertex as playing the role of a trapping center where energy is collected as is the case in the reaction center (RC) of the green sulphur bacteria [25,26], and in which energy conversion occurs.

In order to examine the role of systems parameters such as dissipation rate and time spent at a visited site, we consider the one-dimensional quantum walker for a fixed number of sites. We assume a coin flip operation based on the prototypical dissipation process that takes place during transfer of excitation between two sites $|l\rangle$ and $|m\rangle$

with a total Hamiltonian of the form ($\hbar = 1$)

$$\hat{H}_{ex} = E_l B_l^\dagger B_l + E_m B_m^\dagger B_m + V B_l^\dagger B_m + V B_m^\dagger B_l - i\gamma_l B_l^\dagger B_l - i\gamma_m B_m^\dagger B_m \quad (13)$$

where $B_l^\dagger$ (B_m) is the creation (annihilation) operator of energy of magnitude E_l (E_m) at site l (m). Equation (13) may represent transfer of excited states between neighboring sites in photosynthetic protein complexes of light-harvesting systems and quantum J-aggregates of organic dye molecular systems. V denotes the intersite tunneling energy which is taken to be real and positive, and the dissipative terms γ_l (γ_m) denote the leakage rate of energy at site l (m). Equation (13) can be solved via the retarded Green's function of the form

$$G_{l,m}(t) = -i\Theta(t)\langle\{B_l(t), B_m^\dagger(0)\}\rangle \quad (14)$$

where $\Theta(t)$ denotes a step function. The Fourier transform, $G_{l,m}(E) = \int_{-\infty}^\infty dt\, G_{l,m}(t)\, e^{iEt}$ is given by [48]

$$G_{l,m}^{-1}(E) = \begin{bmatrix} E - E_l + i\eta+ & -V \\ -V & E - E_m + i\eta+ \end{bmatrix} + \frac{i}{2}\begin{pmatrix} \gamma_l & 0 \\ 0 & \gamma_m \end{pmatrix}. \quad (15)$$

where η is a very small number. For an initial state in which the excitation is present only at site l, the probability $P_{l,m}$ of excitation transfer from site l to m is is obtained by inverting Eq. (15)

$$P_{l,m}(t) = \frac{2V^2}{|\Omega|^2} e^{-\gamma_d t}(\cosh \Omega_i t - \cos \Omega_r t), \quad (16)$$

where $\gamma_d = \frac{1}{2}(\gamma_l + \gamma_m)$, $\Omega \equiv \Omega_r + i\Omega_i \equiv \sqrt{4V^2 + (E_0 - i\bar{\gamma}_d)^2}$, $E_0 = E_m - E_l$, $\bar{\gamma}_d = \frac{1}{2}(\gamma_m - \gamma_l)$. The analytical form for the probability, $P_{l,l}(t)$ is lengthy and is not provided here. Simpler expressions can be obtained for the probabilities, $P_{l,m}(t)$ and $P_{l,m}(t)$ at the resonance frequency, $E_0 = 0$, at $E_m = E_l$. At the coherent tunneling regime ($V_0 > \frac{\bar{\gamma}_d}{2}$) we obtain

$$P_{ll} = e^{-\gamma_d t}\left[\cos \Omega_0 t - \frac{\bar{\gamma}_d}{2\Omega_0}\sin \Omega_0 t\right]^2, \qquad P_{lm} = e^{-\gamma_d t}\frac{V^2}{\Omega_0^2}\sin^2 \Omega_0 t, \quad (17)$$

where $\Omega_0 = \sqrt{4V^2 - \bar{\gamma}_d^2}$. The total probabilities, $P_{ll} + P_{lm} \leq 1$ with the loss of normalization dependent on the dissipation terms, γ_d and $\bar{\gamma}_d$. For the case of incoherent tunneling ($V_0 < \frac{\bar{\gamma}_d}{2}$), we replace $\sin[x]$ ($\cos[x]$) by $\sinh[x]$ ($\cosh[x]$). A topological defect occurs at the exceptional point, $\Omega_0 = 0$, $V = \frac{\bar{\gamma}_d}{2}$, which is a unique feature of non-Hermitian quantum systems. At the exceptional point, two eigenvalues of an operator coalesce as a result of a change in system parameters, with the two mutually orthogonal states merging into one self-orthogonal state. We next employ the expressions in Eq. (17) as terms which appear in the non-Hermitian coin flip operation, $\hat{C}'(\alpha)$
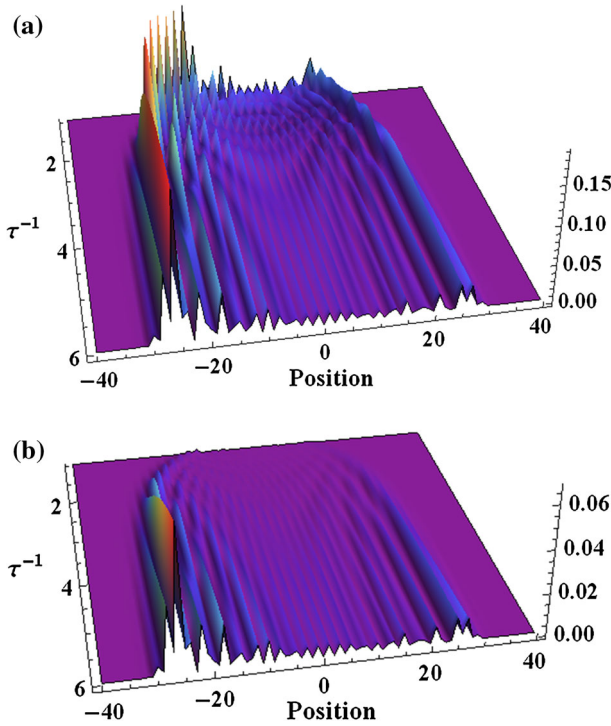
Fig. 2 Probability distribution of a quantum walk (z-axis) as function of position and τ^{-1} obtained after 40 steps at **a** $\lambda = 0$, **b** $\lambda = 0.15$ using the coin operator in Eq. (9) with parameters given in Eq. (18). A unit system in which $\hbar = 1$, $\Omega_0 = 1$ is employed

[see Eq. (9)]

$$\alpha_1 = e^{-\lambda/4\tau} \left[\cos \Omega_0 \tau - \frac{\lambda}{4\Omega_0} \sin \Omega_0 \tau \right], \qquad \alpha_2 = e^{-\lambda/4\tau} \frac{V}{\Omega_0} \sin \Omega_0 \tau \qquad (18)$$

where τ can be considered as the time taken to make one quantum walk. We set $\gamma_m = \lambda$, $\gamma_l = 0$ for simplicity in numerical analysis.

In Fig. 2a, b, we note the spreading out of the probability distribution with decrease in τ, and reduction in probability peaks with introduction of a small dissipation λ =0.15. The reduction is most pronounced at larger $\tau \approx 1$. Figure 3 highlights the nontrivial link between λ and total number of steps taken by the quantum walker. The damping process quantified by λ due to the leakage at each site, acts more effectively when the quantum walk spans a larger number of lattice sites.

It would be worthwhile to discuss the timescales involved during exciton propagation in multi-dimensional systems. Simple estimates obtained using the random walk model by Scheblykin [49], show that the one-dimensional walker is required to visit 10^{11} sites to be quenched by a specific site in a lattice system of 10^6 sites. Assuming the typical exciton lifetime of 100 ps, this implies a waiting time, $\tau \approx 10^{-21}$s at each molecular site. Considering the distance connecting two molecular site to be 1 nm, we
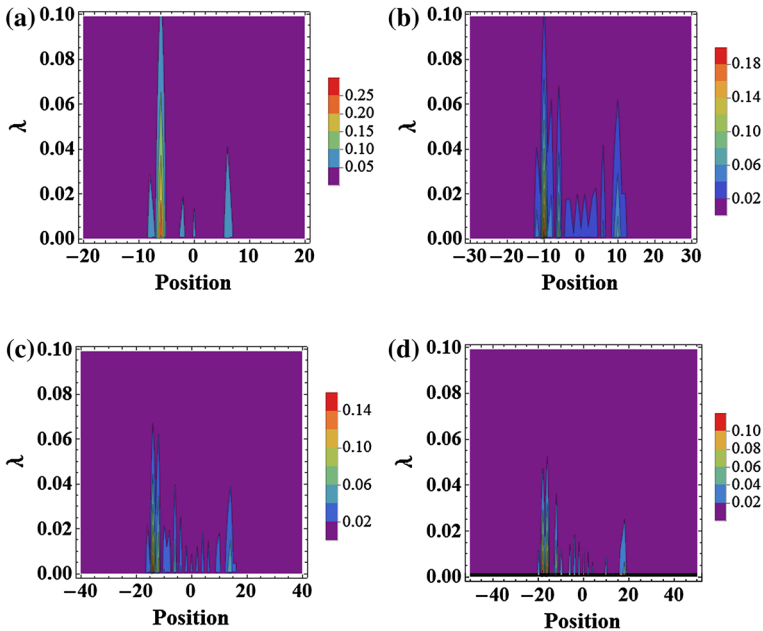
Fig. 3 Probability distribution of a quantum walk as function of position and λ obtained after **a** 20 steps, **b** 30 steps, **c** 40 steps and **d** 50 steps. The coin operator in Eq. (9) with parameters given in Eq. (18) is employed to generate the distribution. τ is set at 1, with $\hbar = 1$ and $\Omega_0 = 1$

would obtain an exciton propagation speed of about 10^{12} m s^{-1} [49], which is higher than the speed of light. To evaluate the lower limit in the exciton speed, we reduce the number of sites visited to 10^6, from which we obtain typical time steps of the order of $\tau \approx 10^{-16}$s, and an exciton speed of propagation of about 10^7 m s^{-1}. These high speeds of propagation (10^7 to 10^{12}) m s^{-1} are best described by the delocalized exciton probing the crystal volume as a massively entangled system with simultaneous feedback mechanisms.

4.1 Non-Hermitian coin flip operation via the exciton spin state

The implementation of the coin operation via the exciton spin dynamics needs some explanation. One approach that can be employed to operate the coin flip operation involves exploiting the spin property of exciton. In molecular systems, the total exciton spin arising from a combination of the electron and hole spin, takes the value of $S = 0$ (singlet state) or $S = 1$ (triplet state)[50]. The singlet state may thus be taken to represent the $|0_c\rangle$ state, while the triplet state may correspond to the $|1_c\rangle$ state

$$|0_c\rangle \equiv |\mathbf{k_e}, \mathbf{k_h}; S = 0\rangle_L = \frac{1}{\sqrt{2}} \left[a_{\mathbf{k_e}}^\dagger (\tfrac{1}{2}) \, c_{\mathbf{k_h}}^\dagger (-\tfrac{1}{2}) - a_{\mathbf{k_e}}^\dagger (-\tfrac{1}{2}) \, c_{\mathbf{k_h}}^\dagger (\tfrac{1}{2}) \right] |0_v\rangle \quad (19)$$

$$|1_c\rangle \equiv |\mathbf{k_e}, \mathbf{k_h}; S = 1\rangle_L = \frac{1}{\sqrt{3}} \left(a_{\mathbf{k_e}}^\dagger (\tfrac{1}{2}) \, c_{\mathbf{k_h}}^\dagger (\tfrac{1}{2}) + a_{\mathbf{k_e}}^\dagger (-\tfrac{1}{2}) \, c_{\mathbf{k_h}}^\dagger (-\tfrac{1}{2}) \right)$$

$$+ \frac{1}{\sqrt{6}} \left(a_{\mathbf{k_e}}^\dagger(-\tfrac{1}{2}) \, c_{\mathbf{k_h}}^\dagger(\tfrac{1}{2}) + a_{\mathbf{k_e}}^\dagger(\tfrac{1}{2}) \, c_{\mathbf{k_h}}^\dagger(-\tfrac{1}{2}) \right) |0_v\rangle \tag{20}$$

where $|0_v\rangle$ denotes the state vector of the vacuum space in which the electron and hole states remain in their respective ground states. The hole (electron) creation operator is denoted by $c_{\mathbf{k_h}}^\dagger$ ($a_{\mathbf{k_e}}^\dagger(\sigma)$) with wavevector $\mathbf{k_h}$ ($\mathbf{k_e}$) and spin, σ. It can be seen that the $S = 0$ spin state of the exciton arises from the coupling of electron with the hole of opposite spins, while the $S = 1$ spin state of the exciton results from the combination of three symmetrical spin functions of the electron and hole spin states with spin components, $S_z = +1, 0, -1$. The $S = 1$ exciton can also be formed due to components, $S_z = +1$ and -1 in the coupling between electron and heavy-hole spin states, but we omit this possibility for brevity of discussion on exciton spin states.

For practical implementations of the coin-flip operation, the differences between the singlet and triplet excitons have to be taken into consideration. The energy of the triplet state is less than the singlet state by 0.5 eV, and have comparatively long diffusion lengths ($\approx 5-10 \times 10^{-6}$m) in organic systems. Moreover energy transfer via Coulomb coupling does not take place in triplet states as the triplet excited state-singlet ground state transition is spin-forbidden. Triplets thus transfer their energy through exchange coupling instead, accordingly the singlet exciton moves faster and decays quickly as well, as it is not subjected to the spin-forbidden decay rule of the triplet state. These differences would introduce "unfairness" during the coin flip operation, which can be minimized if the flip operation is performed within very short time periods lasting 1 fs or less.

The robustness of the coin flip operation $\hat{C}'$ [Eq. (9)] may require further investigation of the Elliot–Yafet (EY) momentum scattering, Elliot–Yafet (EY), Bir–Aroniv–Pikus (BAP) and Dyakonov–Perel (DP) mechanisms, all of which are known to cause spin relaxation of charge carriers [51]. Exciton scattering involving spin-flip processes due to acoustic phonons may also result in spin relaxation processes. A combination of these processes may degrade the coin flip operation $\hat{C}'$, with the decrease in coin flip functionality analyzed by information theoretic measures such as fidelity.

4.2 Von Neumann entropy in the vicinity of the exceptional point

The influence of the time taken to make one quantum walk τ on the dynamics of the quantum walk can be further explored via the widely used von Neumann entropy measure [52]. We modify the expression for the average entropy

$$S = \frac{1}{N} \sum_{n=1}^{N} -\text{Tr}_n \rho_n \ln \rho_n \tag{21}$$

by setting N as the total number of steps taken by the quantum walker. ρ_n is determined using the probability of occupation at site n. A large entropy, S implies substantial entanglement between various sites, while small values of S indicates the presence
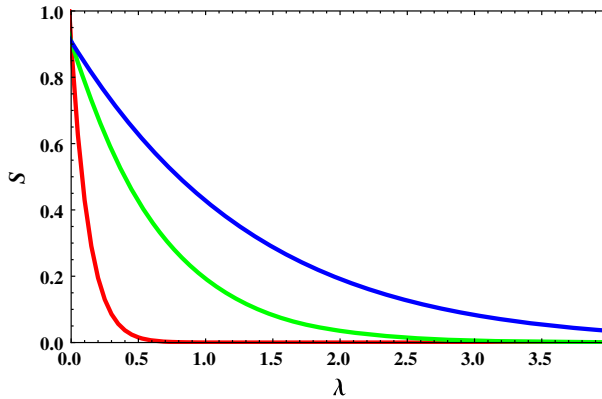
Fig. 4 Average von Neumann entropy of a quantum walk as a function of λ obtained for $\tau = \frac{1}{5}$ (*red line*), $\tau = \frac{1}{25}$ (*green line*) and $\tau = \frac{1}{50}$ (*blue line*). The number of steps taken is fixed at 50 in all three cases (Color figure online)

of a localized state. The entropy measure is therefore useful in characterizing quantum phase transitions at the localization-delocalization boundary. The von Neumann entropy measure can reveal variations in entanglement properties as the exciton propagates in a dissipative environment as shown in Fig. 4. The figure shows the gradual decrease in entropy associated with increased localization at large τ, the time taken to make one quantum walk. This is expected, as the longer time spent at a site results in greater dissipation of energy via a combination of processes that determine the coherence of the exciton state. Processes which govern the excitonic coherence may include exciton-phonon interactions, decoherence due to lattice vibrations at increased temperatures, spin relaxation mechanisms and Pauli interactions [42]. Figure 4 shows that S vanishes at the exceptional point ($\lambda = 4$), reflecting the increased localization effects in the vicinity of topological defects. These results indicate that a small τ correspond to more efficient exciton propagation in photosynthetic systems, and show that dissipative sinks favor the formation of topological defects.

5 Exciton dynamics and quantum tomography

Quantities representing entanglement are determined using quantum states obtained via quantum tomographic methods [52,53]. The term "tomography" is associated with techniques of estimating quantum states to a high degree of accuracy via reconstruction of density matrices. In quantum state tomography (QST), density matrices are estimated using measurement techniques that provide information about the quantum state which may be in a pure or mixed state. By repeated measurements on quantum systems, the derived frequency counts can be used to compute probabilities that assist in building the density matrix of a quantum state. In quantum process tomography (QPT), a priori quantum states are employed to investigate quantum processes. Several works [54–56] have focussed on quantum measurements which can be used to retrieve some or all of the information about a quantum state that is sufficient to quan-

tify entanglement under specific conditions. For the quantum walker in which coin and position states are entangled, we evaluated entanglement through the Von-Neumann entropy in Fig. 4. It was shown that small values of the walk time, τ, and damping factor, λ can contribute to conditions under which entanglement is maximally enhanced. It remains to be seen whether these parameters play important roles during quantum tomography.

The crosspeaks in 2D electronic spectra are proportional to the dipole strength cross-correlation function between exciton states [57]. This feature provides some advantage in tracking excitation propagation on a femtosecond timescale [58]. Recently, exciton relaxation of about 50 fs was observed as an off-diagonal signature in the low-energy cross-peak region of 2D coherent electronic spectral results [45] of molecular aggregate systems. Interestingly inter-band coherence spectroscopic signatures appeared at the same time, and correlated exciton states were projected as off-diagonal signals in the frequency-frequency correlation spectra with a time resolution of about 20 fs [45]. These temporal features on a femtosecond timescale in the sequential 2D electronic spectra highlight the possibility of reconstructing time evolutions of the exciton density matrix in the quantum kinetics regime. The reconstruction procedure constitutes an important aspect of quantum process tomography (QPT) [43,44,46], during which details of the input/output quantum state amplitudes in the excitonic subspace are elucidated by combining a range of experimental results. The final outcome is subsequently derived by varying polarization and frequency components of input pulses.

We note that quantum information processing offers the distinct advantage of dealing with exciton basis that may span over a wide and possibly intricately connected network of molecular sites. This occurs in large photosynthetic membranes, which may link many biomolecular chromophores, and possibly thousands of entangled excitonic qubits in the Hamiltonian subspace. To this end, we focus on two signatures of exciton dynamics that may be observed via a quantum information theoretic approach to spectroscopic experiments. The first attribute useful to understanding the correlated dynamics in excitonic systems relates to the presence of topological defects such as exceptional points. In a recent work [33], we showed the appearance of exceptional points in non-Hermitian excitonic dimers during excitation energy transfer for a select range of temperatures and damping parameters. The second attribute involves the salient feature of non-Markovianity, whose measures are based on deviations from the continuous, memoryless, completely positive semi-group feature of Markovian evolution of quantum systems [59,60]. Non-Markovian dynamics appear to be a necessary aspect of quantum dynamics of open quantum systems when the commonly used Markovian model breaks down in the presence of strong system-environment coupling regime or preexisting unfactorized initial conditions between the system and environment.

The role of the exceptional point and non-Markovian dynamics can be examined in the context of a quantum walk governed by a non-Hermitian coin flip operation. During an excitonic quantum walk, the number of qubits that exist within the total Hilbert space, $\mathcal{H}_w = \mathcal{H}_p \otimes \mathcal{H}_c$ increases beyond computational tractability of non-Markovian features, even for steps taken over five or more bacteriochlorophyll (BChl)a molecules sites of the FMO complex monomer subunit. Moreover the number of

Table 1 Outcome of quantum measurements after two steps of a quantum walk

Probability	Measurement	State
$\frac{\alpha_1^4}{4\beta^2}$	$\{0_c \ -2_p\}$	$|0_c\rangle \otimes |-2_p\rangle$
$\frac{\alpha_1^2\alpha_2^2}{4\beta^2}$	$\{0_c \ -1_p\}$	$-|0_c\rangle \otimes |-1_p\rangle$
$\frac{1}{\beta^2}\left(\frac{\alpha_1^2}{2}+\alpha_2^2\right)^2$	$\{0_c \ 0_p\}$	$|0_c\rangle \otimes |0_p\rangle$
$\frac{\alpha_1^2\alpha_2^2}{4\beta^2}$	$\{0_c \ 1_p\}$	$|0_c\rangle \otimes |1_p\rangle$
$\frac{\alpha_1^4}{4\beta^2}$	$\{1_c \ -1_p\}$	$|1_c\rangle \otimes |-1_p\rangle$
$\frac{\alpha_1^2\alpha_2^2}{4\beta^2}$	$\{1_c \ 0_p\}$	$|1_c\rangle \otimes |0_p\rangle$
$\frac{\alpha_1^4}{4\beta^2}$	$\{1_c \ 1_p\}$	$-|1_c\rangle \otimes |1_p\rangle$
$\frac{\alpha_1^2\alpha_2^2}{4\beta^2}$	$\{1_c \ 2_p\}$	$-|1_c\rangle \otimes |2_p\rangle$

$\beta^2 = \left(\alpha_1^2 + \alpha_2^2\right)^2$ where α_1, α_2 appear as elements in the non-Hermitian coin flip operator $\hat{C}'$ [see Eq. (9)]. The degree of dissipation of the system undergoing non-Hermitian dynamics is determined by the difference $\Delta = \alpha_1 - \alpha_2$

quantum measurements required to tract the qubit dynamics also increases steeply with the number of qubits. We therefore confine our analysis to the quantum walk which ends at $N < 6$ steps.

During quantum measurements of a system $\mathcal{S}$, values of a physical quantity is transferred to a monitoring device $\mathcal{M}$, with the mapping $\mathcal{S} \rightarrow \mathcal{M}$ representing a mathematical description of the measurement. It is considered that the quantum states of the monitoring device can be easily read, and that these quantum states are orthogonal to one another, with fulfillment of the normalization condition. There are several ways to extract information from the coin-position composite state arising from the quantum walk. For instance, we may first perform a measurement on the coin using the observable of the form $\hat{O}_c = \gamma_0|0\rangle_c\langle0| + \gamma_1|1\rangle_c\langle1|$. A second measurement is next performed on the position states via the operator $\hat{O}_p = \sum_i \alpha_i|i\rangle_p\langle i|$. In Table 1 we provide results of quantum measurements of the quantum walk after $N = 2$ steps, obtained using "Quantum", the package for Dirac Notation in Mathematica. Since only the diagonal elements are retrieved, there is insufficient information to fully characterize the entanglement and non-classical correlation aspects of the exciton dynamics. The diagonal terms however, will suffice to provide useful information related to the exceptional point. We use as basis the exemplary exciton transfer process between two sites as described by the total Hamiltonian in Eq. (13), and the occupation probabilities in Eq. (18). We evaluate the measurement based profiles of various quantum states as recorded by the monitoring system (shown in Fig. 5a, b) in the vicinity of the exceptional point which occurs when the dissipative measure, $\lambda \rightarrow 4$. The probabilities are based on the results of the quantum measurements given in Table 1, at two different times needed to make a quantum step. The profiles show the increased probability (due to localization) to remain at the starting point of quantum walk for longer time steps ($\tau = 0.5$) as compared to shorter

time steps($\tau = 0.1$). As expected, a different measurement profile (Fig. 5c, d) is obtained when the outcome is recorded after five steps of the quantum walk. These results indicate that the conditions under which topological defects occur could be determined by comparing differences in site occupation probabilities as the environmental settings are varied. Exceptional points are generally associated with a range of system parameter attributes, and thus a spectrum of defects may be detected through experiments. This approach provides an indirect technique of probing the quantum dynamical processes and transitions which may occur in the femtosecond timescale, as the typical $\tau \approx 1$ fs.

There is also possibility of observing phase transitions via time series-type tomographic techniques using ultrafast spectroscopy experiments. The actual implementation of experimental techniques is beyond the scope of this work as measurement procedures are non-ideal [61] and the density matrix of a probed system is susceptible to noise related errors. One may employ algorithmic procedures such as the Maximum Entropy estimation [62], or the Variational Quantum Tomography (VQT) [63] which involves the minimization of a linear cost function. These approaches may help in the estimation of density matrices with higher accuracy, and the dissipative conditions under which exceptional points and phase transitions may occur.

5.1 Non-Markovianity during quantum walk

We examine the complex interplay of non-Markovian signatures that occur in the total Hilbert space, when quantum measurements are performed during the quantum walk. The regeneration of a density matrix from an unknown state involves measurement projections of density matrices which are Hermitian, of unity trace, and which obey the positivity conditions [59]. The density matrix is obtained by projecting the unknown quantum state onto a set of known states derived from experimental results. However the interference effects between coin and walker coupled with interaction of the coin with the environment, may give rise to non-Markovian effects which violates positivity conditions during the quantum walk.

The trace distance $D[\rho_1, \rho_2]$ [64] is a well known metric measure of distinguishability of two quantum states ρ_1, ρ_2 and is computed using $D[\rho_1, \rho_2] = \frac{1}{2}||\rho_1 - \rho_2||$ [52] where $||A|| = Tr[\sqrt{A^\dagger A}]$ between ρ_1, ρ_2. During Markovian evolutions, the trace-distance does not increase with time and $D[\rho_1(t), \rho_2(t)] < D[\rho_1(0), \rho_2(0)]$. The violation of this inequality signals the breakdown of the complete positivity condition during the time-evolution of a quantum system. It is to be noted that an increase of trace distance during a time intervals is a sufficient but not necessary indication of the occurrence of non-Markovianity. In this work, we employ the trace-distance difference

$$D(T, \tau) = D[\rho(\tau'), \rho(\tau)] - D[\rho(T + \tau'), \rho(T + \tau)], \qquad (23)$$

where $\tau' << \tau$, to identify non-Markovian dynamics during the entangled quantum walk.

(a)

(b)

(c)

(d)
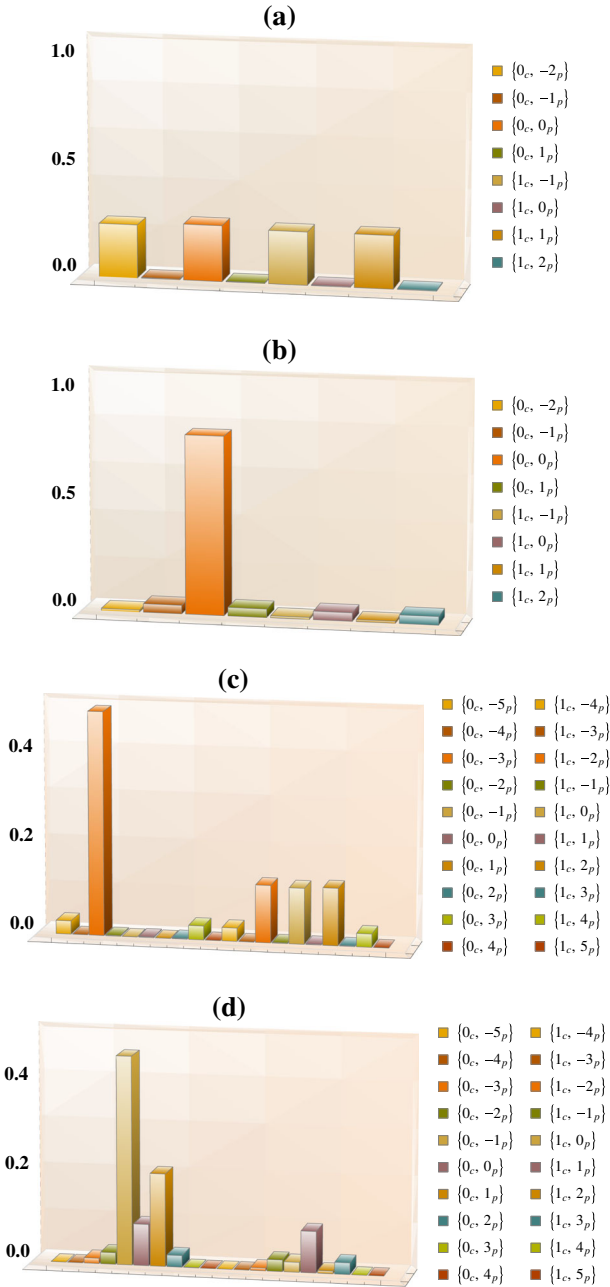
Fig. 5 Measurement profiles of various quantum states as recorded by the monitoring system for $\lambda \approx$ 3.9, in the vicinity of the exceptional point for **a** $\tau = 0.1$, **b** $\tau = 0.5$ evaluated for a quantum walk that terminates after 2 steps, and **c** $\tau = 0.1$, **d** $\tau = 0.5$ evaluated for a quantum walk that terminates after 5 steps. A unit system in which $\hbar = 1$, $\Omega_0 = 1$ is employed. Units for time τ (time taken to make a single step) is based on the inverse of Ω_0 (at $\lambda = 0$). τ can be interpreted as inversely proportional to the exciton diffusion speed
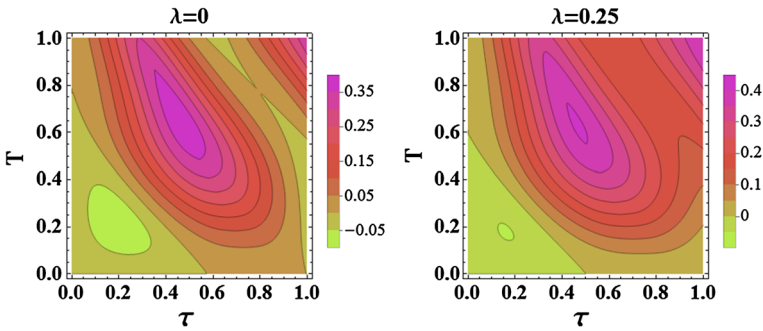
Fig. 6 Trace-distance difference function, $D(T, \tau)$ [Eq. (23)] as a function of the time of one quantum step, τ and the lapse time, T. $D(T, \tau)$ is based on the reduced density matrix describing the quantum walk in the position basis [see Eq. (24)]. The shading in the bar-legend identifies regions undergoing non-Markovian dynamics (negative values of $D(T, \tau)$). Values of λ are indicated at the top of each figure and and $\tau' = 0.00001$. The unit system is based on $\hbar = V = 1$, with time t obtained as inverse of Ω_0 (at $\lambda = 0$)

For computational simplicity, we consider the case of the quantum walk which terminates after $N = 2$ steps. By tracing out the coin states of the walker, we obtain a reduced density matrix describing the quantum walk in the position basis $(\left|-2_p\right\rangle, \left|-1_p\right\rangle, \left|0_p\right\rangle, \left|1_p\right\rangle, \left|2_p\right\rangle)$

$$\rho_p(\alpha_1, \alpha_2) =$$

$$
\begin{pmatrix}
\frac{\alpha_1^4}{4} & -\frac{1}{4}\alpha_1^3\alpha_2 & \frac{1}{2}\alpha_1^2\left(\frac{\alpha_1^2}{2}+\alpha_2^2\right) & \frac{1}{4}\alpha_1^3\alpha_2 & 0 \\
-\frac{1}{4}\alpha_1^3\alpha_2 & \frac{\alpha_1^4}{4}+\frac{1}{4}\alpha_2^2\alpha_1^2 & \frac{1}{4}\alpha_1^3\alpha_2-\frac{1}{2}\alpha_1\alpha_2\left(\frac{\alpha_1^2}{2}+\alpha_2^2\right) & -\frac{\alpha_1^4}{4}-\frac{1}{4}\alpha_2^2\alpha_1^2 & -\frac{1}{4}\alpha_1^3\alpha_2 \\
\frac{1}{2}\alpha_1^2\left(\frac{\alpha_1^2}{2}+\alpha_2^2\right) & \frac{1}{4}\alpha_1^3\alpha_2-\frac{1}{2}\alpha_1\alpha_2\left(\frac{\alpha_1^2}{2}+\alpha_2^2\right) & \frac{1}{4}\alpha_1^2\alpha_2^2+\left(\frac{\alpha_1^2}{2}+\alpha_2^2\right)^2 & \frac{1}{2}\alpha_1\alpha_2\left(\frac{\alpha_1^2}{2}+\alpha_2^2\right)-\frac{1}{4}\alpha_1^3\alpha_2 & -\frac{1}{4}\alpha_1^2\alpha_2^2 \\
\frac{1}{4}\alpha_1^3\alpha_2 & -\frac{\alpha_1^4}{4}-\frac{1}{4}\alpha_2^2\alpha_1^2 & \frac{1}{2}\alpha_1\alpha_2\left(\frac{\alpha_1^2}{2}+\alpha_2^2\right)-\frac{1}{4}\alpha_1^3\alpha_2 & \frac{\alpha_1^4}{4}+\frac{1}{4}\alpha_2^2\alpha_1^2 & \frac{1}{4}\alpha_1^3\alpha_2 \\
0 & -\frac{1}{4}\alpha_1^3\alpha_2 & -\frac{1}{4}\alpha_1^2\alpha_2^2 & \frac{1}{4}\alpha_1^3\alpha_2 & \frac{1}{4}\alpha_1^2\alpha_2^2
\end{pmatrix}
$$

$$(24)$$

where α_1, α_2 appear as elements in the non-Hermitian coin flip operator $\hat{C}'$ in Eq. (9). We compute the trace-distance difference [Eq. (23)] for a quantum walk with a coin flip operator $\hat{C}'$ based on the exciton occupation probabilities in Eq. (18) and the reduced density matrix in Eq. (24).

Figure 6 illustrates the trace-distance difference, $D(T, \tau)$ [Eq. (23)] as a function of the time for one quantum step, τ and the lapse time, T for the reduced density matrix associated with a quantum walk that terminates after two steps [see Eq. (24)]. The figure show regions undergoing non-Markovian dynamics (negative values of $D(T, \tau)$) at small values of τ, $T \approx 0.2$, which is optimized at $\lambda = 0$. The non-Markovian dynamics therefore dominates at the initial period of quantum evolution, at times of the order of the environmental bath memory time. The sensitivity of the qubit dynamics to the dissipation measure λ is highlighted by Fig. 6b. An increase

in λ suppresses non-Markovian dynamics, we therefore expect the qubit dynamics (in position basis) to become Markovian beyond a critical dissipation λ_c. This is consistent with diminished population exchanges between the quantum walker and the dissipative environment at each lattice sites, as also seen by the decrease of the von Neumann entropy measure in Fig. 4. While the results obtained in Fig. 6 is specific to the 5×5 reduced density matrix in Eq. (24), similar features of information back-flow are expected for quantum walks terminating after higher number of steps.

Variations in non-Markovian dynamics may appear with further expansion of the quantum walk to two or three dimensions, and the inclusion of greater degree of topological connectivity at each visited site. These features are more representative of the realistic molecular structures in multi-chromophoric macromolecule systems. The analysis of non-Markovian dynamics in large networks of molecular systems would however involve greater computational times. To this end, it would be worthwhile to examine the possibility of tracking non-Markovian type processes through resurgence of signatures of population dynamics in the initial quantum kinetic time regime via quantum tomography schemes. Exciton coherence structures are known to be associated with quantum beat oscillations in the initial time period of about 100 fs [45]. In contrast streaked signals become superposed on the coherence frequency patterns when the exciton relaxes without re-populating. Improvements in current quantum process tomography techniques will enable the detection of non-Markovian dynamics, and provide better understanding of exciton dissipative dynamics that underpins the high efficiencies of energy transfer processes in photosynthetic systems.

6 Conclusion

In this paper, we examine in situ, without resorting to perturbative or other approximation schemes, the coherent propagation of the one-dimensional Frenkel exciton (correlated electron-hole pair system) based a model of a quantum walker in multi-dimensional Hilbert space. The walk is governed by a non-Hermitian coin flip operation which is coupled to a generalized shift operation. The dissipative coin flip operation is associated with the loss of amplitude at newly located site, representative of processes which occur when an exciton is transferred along dimer sites in photosynthetic protein complexes. These processes may include localization effects due to diagonal disorder and decoherence effects arising from thermal vibrations at increasing temperatures. The results obtained in this study show the uniqueness of the non-Hermitian quantum walk approach in analyzing exciton propagation in biomolecular systems.

We further examine the possibilities of extracting topological defects such as exceptional points and non-Markovian features utilizing quantum process tomography techniques. The techniques may involve specific measurements of the excitonic subspace needed to reconstruct the exciton state density matrix spanning several molecular sites, via a series of ultrafast spectroscopic sequences, with simultaneous variation of environmental parameters. Entanglement and quantum correlation measures estimated from the time-evolution characteristics of the density matrix will enable more accurate evaluation of the quenching rate and the exciton diffusion length in solids.

The ability to deduce topological structures, phase transitions and non-Markovian features, with further improvements in optical retrieval techniques, will certainly enhance the information content of spectroscopy results. It is expected that investigations focussed on determining the links between the quantum coherence model used in this work, and protein-induced fluctuations and dissipation processes would provide further insight to the energy transfer dynamics in correlated biomolecular systems. The incorporation of statistical principles based on the linear response theory of fluctuations in the electronic energies of pigments which are embedded in a protein cage environment, and time-dependent reorganization or solvation of proteins within a quantum walk approach, will contribute to further understanding of the dynamics of intricately connected complex molecular systems in the nanoscale limit.

References

1. J. Kempe, Contemp. Phys. **44**, 307 (2003)
2. Y. Aharonov, L. Davidovich, N. Zagury, Phys. Rev. A **48**, 1687 (1993)
3. A. Ambainis, Int. J. Quantum. Inform. **1**, 507 (2003)
4. E. Farhi, J. Goldstone, S. Gutmann, Theor. Comput. **4**, 169 (2008)
5. E. Farhi, S. Gutmann, Phys. Rev. A **58**, 915 (1998)
6. Y. Shikano, J. Comput. Theor. Nanosci. **10**, 1558–1570 (2013)
7. N.B. Lovett, S. Cooper, M. Everitt, M. Trevers, V. Kendon, Phys. Rev. A **81**, 042330 (2010)
8. M.S. Underwood, D.L. Feder, Phys. Rev. A **85**, 052314 (2012)
9. A.M. Childs, Phys. Rev. Lett. **102**, 180501 (2009)
10. D.A. Meyer, J. Stat. Phys. **85**, 551 (1996)
11. Y. Shikano, T. Wada, J. Horikawa, Nonlinear Discrete-Time Quantum Walk and Anomalous Diffusion (2013), arXiv preprint arXiv:1303.3432
12. A. Ahlbrecht, H. Vogts, A.H. Werner, R.F. Werner, J. Math. Phys. **52**, 042201 (2011)
13. P. Xue, B.C. Sanders, Phys. Rev. A **85**, 022307 (2012)
14. C. Ampadu, Commun. Theor. Phys. **57**, 41 (2012)
15. A. Wójcik, T. Luczak, P. Kurzynski, A. Grudka, T. Gdala, M. Bednarska-Bzdega. Phys. Rev. A **85**, 012329 (2012)
16. M. Gönülol, E. Aydiner, Ö.E. Müstecaplioglu, Phys. Rev. A **80**, 022336 (2009)
17. S. Attal, F. Petruccione, C. Sabot, I. Sinayskiy, J. Stat. Phys. **147**(4), 832–852 (2012)
18. A. Schreiber, K.N. Cassemiro, V. Potocek, A. Gbris, I. Jex, Ch. Silberhorn, Phys. Rev. Lett. **106**, 180403 (2011)
19. A. Ahlbrecht, V.B. Scholz, A.H. Werner, J. Mat. Phys. **52**, 102201 (2011)
20. J.P. Keating, N. Linden, J.C.F. Matthews, A. Winter, Phys. Rev. A **76**, 012315 (2007)
21. M.A. Broome, A. Fedrizzi, B.P. Lanyon, I. Kassal, A. Aspuru-Guzik, A.G. White, Phys. Rev. Lett. **104**, 153602 (2010)
22. R. Matjeschk, M. Ch Schneider, T.H. Enderlein, New J. Phys. **14**, 035012 (2012)
23. L. Sansoni, F. Sciarrino, G. Vallone, P. Mataloni, A. Crespi, R. Ramponi, R. Osellame, Phys. Rev. Lett. **108**, 010502 (2012)
24. G.S. Engel, T.R. Calhoun, E.L. Read, T.-K. Ahn, T. Mancal, Y.-C. Cheng, R.E. Blankenship, G.R. Fleming, Nature **446**, 782 (2007)
25. J. Adolphs, T. Renger, Biophys. J. **91**, 2778 (2006)
26. H. Lee, Y.-C. Cheng, G.R. Fleming, Science **316**, 1462 (2007)

27. C. Olbrich, T.L.C. Jansen, J. Liebers, M. Aghtar, J. Strümpfer, K. Schulten, J. Knoester, U.J. Kleinekathöefer, Phys. Chem. B **115**, 8609 (2011)
28. F. Caruso, A.W. Chin, A. Datta, S.F. Huelga, M.B. Plenio, Phys. Rev. A **81**, 062346 (2010)
29. F. Caruso, A.W. Chin, A. Datta, S.F. Huelga, M.B. Plenio, J. Chem. Phys. **131**, 105106 (2009)
30. M. Mohseni, P. Rebentrost, S. Lloyd, A. Aspuru-Guzik, J. Chem. Phys. **129**, 174106 (2008)
31. A. Ishizaki, G.R. Fleming, Proc. Natl. Acad. Sci. USA **106**, 17255 (2009)
32. J. Wu, F. Liu, Y. Shen, J. Cao, R.J. Silbey, New J. Phys. **12**, 105012 (2010)
33. A. Thilagam, J. Chem. Phys. **136**, 065104 (2012)
34. A. Thilagam, J. Chem. Phys. **136**, 175104 (2012)
35. S.F. Huelga, M.B. Plenio, Vibrations, quanta and biology. Contemp. Phys. **54**, 181–207 (2013)
36. A. Thilagam, Natural Light Harvesting Systems: Unraveling the Quantum Puzzles (2013). arXiv preprint arXiv:1310.7761
37. P. Rebentrost, M. Mohseni, A. Aspuru-Guzik, J. Phys. Chem. B **113**, 9942 (2009)
38. A. Thilagam, J. Chem. Phys. **138**, 175102 (2013)
39. I. Rotter, A.F. Sadreev, Phys. Rev. E **71**, 03622 (2005)
40. M. Combescot, O. Betbeder-Matibet, F. Dubin, Phys. Rep. **463**, 215 (2008)
41. A. Thilagam, J. Math. Chem. **51**, 1897 (2013)
42. A. Thilagam, Phys. Rev. B **59**, 3027 (1999)
43. Y.S. Weinstein, T.F. Havel, J. Emerson, N. Boulant, M. Saraceno, S. Lloyd, D.G. Cory, J. Chem. Phys. **121**, 6117–6133 (2004)
44. T.J. Dunn, I.A. Walmsley, S. Mukamel, Phys. Rev. Lett. **74**, 884 (1995)
45. F. Milota, J. Sperling, A. Nemeth, H.F. Kauffmann, Chem. Phys. **357**, 45 (2009)
46. L. Zhang, H.B. Coldenstrodt-Ronge, A. Datta, G. Puentes, J.S. Lundeen, X.-Min Jin, B.J. Smith, M.B. Plenio, I.A. Walmsley, Nat. Photonics **6**, 364 (2012)
47. A. Thilagam, Phys. Rev. A **81**, 032309 (2010)
48. B.A. Lippmann, J. Schwinger, Phys. Rev. **79**, 469 (1950)
49. I.G. Scheblykin, Chapter 9, pg. 247 of Takayoshi Kobayashi. J-Aggregates, vol. 2 (World Scientific, Singapore, 2012)
50. A. Thilagam, M.A. Lohe, J. Phys.: Condens. Matter **18**, 3157 (2006)
51. G. Pikus, A. Titkov, *Spin Relaxation Under Optical Orientation in Semiconductors Optical Orientation* (North-Holland, Amsterdam, 1984)
52. M.A. Nielsen, I.L. Chuang, *Quantum Computation and Quantum Information* (Cambridge University Press, Cambridge, 2002)
53. M. Mohseni1, A.T. Rezakhani, D.A. Lidar, Phys. Rev. A **77**, 032322 (2008)
54. O. Gühne, G. Toth, Phys. Reports **474**, 1 (2009)
55. G. Toth, O. Gühne, Phys. Rev. Lett. **94**, 060501 (2005)
56. K.M.R. Audenaert, M.B. Plenio, New J. Phys. **8**, 266 (2006)
57. M. Cho, Chem. Rev. **108**, 1331 (2008)
58. J.R. Caram, A.F. Fidler, G.S. EngeL, J. Chem. Phys. **137**, 024507 (2012)
59. E.C.G. Sudarshan, P.M. Mathews, J. Rau, Phys. Rev. **121**, 920 (1961)
60. M. Choi, Positive linear maps on C*-algebras. Can. J. Math **24**(3), 520–529 (1972)
61. A. Thilagam, J. Phys. A: Math. Theor. **45**, 444031 (2012)
62. V. Buzek, G. Drobny, R. Derka, G. Adam, H. Wiedemann, Chaos Solitons Fractals **10**, 981 (1999)
63. T.O. Maciel, A.T. Cesario, R.O. Vianna, Int. J. Mod. Phys. C **22**, 1361 (2011)
64. H.-P. Breuer, E.-M. Laine, J. Piilo, Phys. Rev. Lett. **103**, 210401 (2009)